

# Dynamics of wave-induced currents over an alongshore non-uniform multiple-barré sandy beach on the Aquitanian Coast, France

Bruno Castelle\*, Philippe Bonneton, Nadia Sénéchal, H el ene Dupuis,  
R emi Butel, Denis Michel

*Department of Geology and Oceanography, UMR CNRS 5805 EPOC, University of Bordeaux I, 33405 Talence cedex, France*

Received 9 April 2004; received in revised form 11 August 2005; accepted 23 August 2005  
Available online 15 November 2005

## Abstract

This paper presents field investigation and numerical modelling of waves and wave-induced currents on a wave-dominated and non-alongshore uniform multiple barr e beach. This study aims at establishing the first analysis of the dynamics of horizontal flows on the French Aquitanian coast. The spectral wave program SWAN is coupled with the time- and depth-averaged (2DH) coastal area model MORPHODYN. This coupled-model is applied to Truc Vert Beach, and results are compared with field data. From the 14th to the 19th of October 2001, a field experiment was carried out in order to characterize hydrodynamics and sediment transport over a complex bathymetry in the presence of oceanic wave conditions. From this data we calibrated three parameters: the bottom friction for wave propagation from the Aquitanian continental shelf to the nearshore zone, the spatially constant bottom friction coefficient due to waves and currents, and lateral mixing. Despite model approximations and the fact that the offshore wave boundary condition was located 15 km off the coast, the model is in good agreement with measurements. During weak wind conditions, computed waves and longshore currents fit well with field data on the ridge and runnel system. The strong tidal modulation of surf zone processes over this system is revealed. Hydrodynamics are strongly controlled by the beach morphology. For near-normally incident swells, the ridge and runnel system is responsible for a strong rip current located at the runnel outlet, associated with a circulation cell. Prediction of the tidal modulation and the sensitivity of the rip current to offshore wave conditions are in agreement with observations. Maximum rip current flow velocities occur approximately at mid-tide, which differs from what most researchers have found in other environments.

  2005 Elsevier Ltd. All rights reserved.

*Keywords:* France; Aquitanian coast; Nearshore dynamics; Rip currents; Longshore current; Field measurements; Modelling; Ridge and runnel system

## 1. Introduction

Ocean waves are the primary cause of sediment transport and morphological change in the nearshore. During the past three decades, knowledge of the physical processes related to waves, wave-induced currents and sediment transport has

\*Corresponding author. Now at Griffith Centre for Coastal Management, Gold Coast, Australia. Tel.: +61 (0)7 5552 8520; fax: +61 (0)7 5552 8067.

*E-mail address:* [b.castelle@griffith.edu.au](mailto:b.castelle@griffith.edu.au) (B. Castelle).

improved. However, on natural beaches, accurate prediction of wave-induced current circulations which control the nearshore sediment transport rate remains an open issue. In particular, the determination of longshore current structure and rip current behaviour are important topics for further research. In this paper, waves and wave-induced currents are investigated using measurements and numerical modelling over the Aquitanian beaches, which have not received much attention in the literature previously. In this environment, the longshore non-uniform topography and wave climate are responsible for complex rip currents, nearshore cell circulations and longshore currents. These are discussed herein and compared with other environments.

Cross-shore variability and magnitude of longshore currents have been investigated for a long time using different approaches. Laboratory experiments were undertaken by Visser (1991), Hamilton and Ebersole (2001) among others, to improve methods for predicting wave-induced currents and nearshore sediment transport rates. For barred and planar beaches, laboratory experiments show that the maximum longshore current velocity is located where breaking is most intense, i.e. on the bar and near the shoreline. Early longshore current models were reduced to one dimension (Longuet-Higgins, 1970) and predict the magnitude and location of the maximum longshore current at the breaking point. For alongshore uniform barred-beaches, the maximum of longshore current can be expected to occur at the point of most intense wave breaking (Ruessink et al., 2001; Feddersen and Guza, 2003), i.e. on the bar, consistent with the laboratory results of Reniers and Battjes (1997). When a barred-beach has strong alongshore non-uniformities, the maximum of longshore current is located in the trough (Church and Thornton, 1993; Kuriyama and Nakatsukasa, 2000). Several mechanisms were examined to explain this spatial lag. Roller effects on the longshore distribution were investigated by Reniers and Battjes (1997) as well as turbulent eddy viscosity. Church and Thornton (1993) examined the effects of wave-induced turbulence on the bottom shear stress and resulting longshore current profiles. However, the longshore pressure gradient due to longshore bathymetry inhomogeneities is the only mechanism able to shift enough the velocity maximum away from the bar crest (Petrevu et al., 1995; Reniers and Battjes, 1997; Feddersen et al., 1998).

The rip current is another common horizontal flow pattern which occurs on natural beaches. Rips

are strong and narrow seaward oriented currents, responsible for significant sediment transport (Cook, 1970; Inman et al., 1971; Brander, 1999) and morphology change in the nearshore (Sonu, 1972; Short, 1979, 1992; Wright and Short, 1984). Recently, field studies have been undertaken to improve knowledge of this nearshore circulation pattern (Aagaard et al., 1997; Brander, 1999; MacMahan et al., 2003). The tidal modulation of the rip current velocity, with maximum velocities occurring at low-tide, were investigated by Brander (1999). A first scaling relationship between incoming waves and rip current dimension was established by Brander (2000). Haas and Svendsen (2002) investigated the vertical structure of the rip current from laboratory experiments in comparison with quasi-3D numerical simulations. They found that the vertical profile of the rip current varies from a depth uniform pattern in the channel to depth varying pattern further offshore, with maximum velocity at the surface.

The present study aims at investigating the structure and magnitude of longshore current and rip currents on a type of beach which behaves differently than others reported in the literature. The French Aquitanian coast beaches exhibit strongly longshore non-uniform multiple bars, resulting in complex horizontal wave-induced current patterns which are poorly understood. The lack of data is due both to a very energetic wave climate and difficult access to the study area, which makes intensive measurements in the field a challenging task, particularly in the shallow subtidal zone. Before PNEC 2001 experiment, measurements of rips and nearshore cell circulation were few, and virtually non-existent in the environment described in this paper. The present study paves this gap with a quality dataset. Combination of modelling, field measurements analysis and satellite imagery is used to investigate the random wave transformation and wave-induced currents. A two-dimensional depth-averaged motion approach (2DH) is undertaken to predict longshore current structure and rip currents. The two-dimensional structure, magnitude, tidal modulation and sensitivity to offshore wave conditions of wave-induced currents are then analysed.

## 2. Study area

The French Aquitanian coast is a 230 km high energy meso-macrotidal straight coast between the Gironde estuary and the Adour estuary (Fig. 1).

The high meso-macro tidal range is about 5 m at spring tides, along with a relatively broad intertidal region of approximately 200 m. This coast is bordered by high aeolian dunes and the sediment consists of fine to medium sand ( $200 \mu\text{m} < d_{50} < 350 \mu\text{m}$ ). The coast is exposed to almost continuous high energy swells. Statistical analysis of non-directional Datawell wave rider times series (in 26 m water depth) shows that this coast is mainly concerned by very low steepness swell waves (mean annual  $H_s$  and period of 1.4 m and 6.5 s), travelling mainly from W–NW directions (Butel et al., 2002). During storms, offshore significant wave height can reach 10 m. The mean wave incidence induces a strong southerly longshore drift (Michel and Howa, 1994). In the area situated outside the influence of the Arcachon lagoon and Gironde estuary, tidal currents are not significant in comparison with wave-induced currents.

Following the beach state classification of Short (1992) and Short and Aagaard (1993), Aquitanian coast beach state is mainly an intermediate (d) double-barred beach. The nearshore is characterized by two distinct sand bar patterns: the crescentic bar system in the subtidal zone and the ridge and runnel system in the intertidal zone (Michel and Howa, 1999). After long periods of fair weather conditions, ridges are regularly interrupted by down-current oriented runnels with a mean wavelength of about 400 m (year-average), i.e. a rip density (RD) of 2.5. This value of RD characterizes west coast swell environments (Short and Brander, 1999), going against the world wave environment classification of Davies (1980) in which the Aquitanian coast is defined as a storm wave environment. Fig. 2 shows an aerial view of a ridge and runnel system on the Aquitanian Coast. Rip channel migration is about 3 m per day during summer (Lafon et al., 2002). After the occurrence of high energy wave conditions, random direction runnels with a large range of rip spacing are observed. The nearshore zone exhibits large scale crescentic bars (Froidefond et al., 1990) whose shape can vary from typically crescentic to a seldom observed lunate shape with a mean wavelength of about 700 m (Lafon et al., 2005). Fig. 3 shows a SPOT image of a regular nearshore crescentic bar system from Truc Vert Beach to the end of the sand spit. Sometimes a third bar system inshore of the crescentic bars can be connected to the ridge and runnel system. This system has a crescent shape, and it results in a shifting of the beach state to intermediate (e)

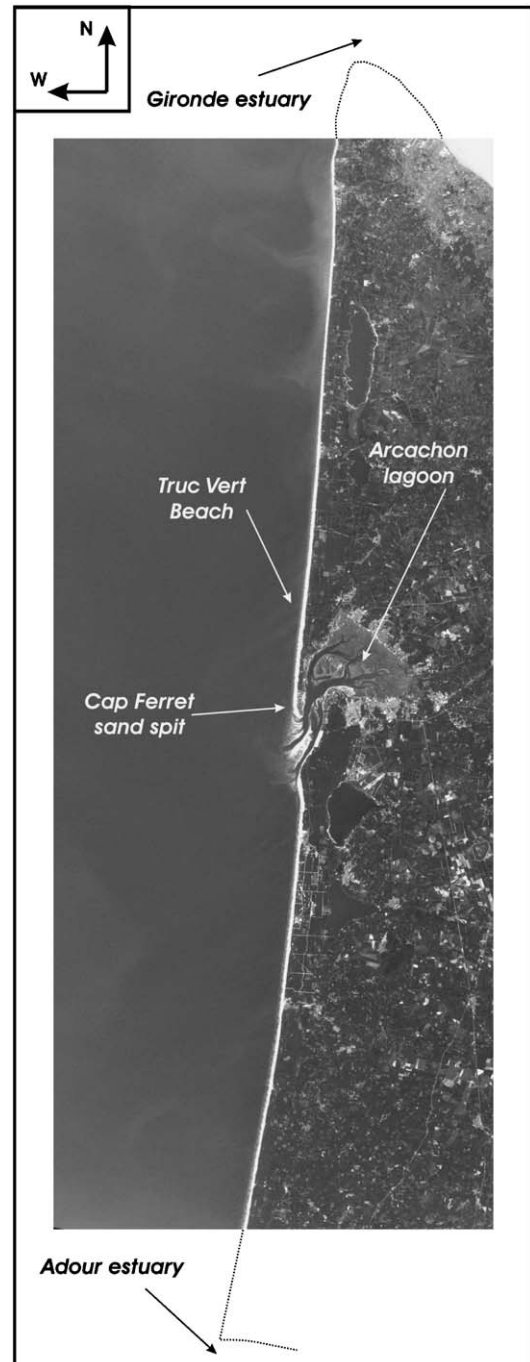


Fig. 1. Satellite image (SPOT XS1) of the Aquitanian Coast between the Gironde estuary and the Adour estuary. Location of Truc Vert Beach on the upper part of the Cap Ferret sand spit.

following the classification of Short (1992). The morphodynamics of these intertidal and nearshore bar systems are still not well understood, and a state of the art of our knowledge is given by Castelle et al. (2005).

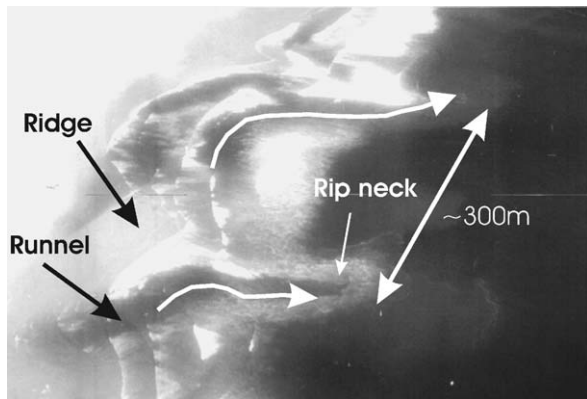


Fig. 2. Aerial photograph of a regular ridge and runnel system in the intertidal domain, Aquitanian Coast. Location of rip currents located at the runnel outlets with two sediment plumes is highlighted.

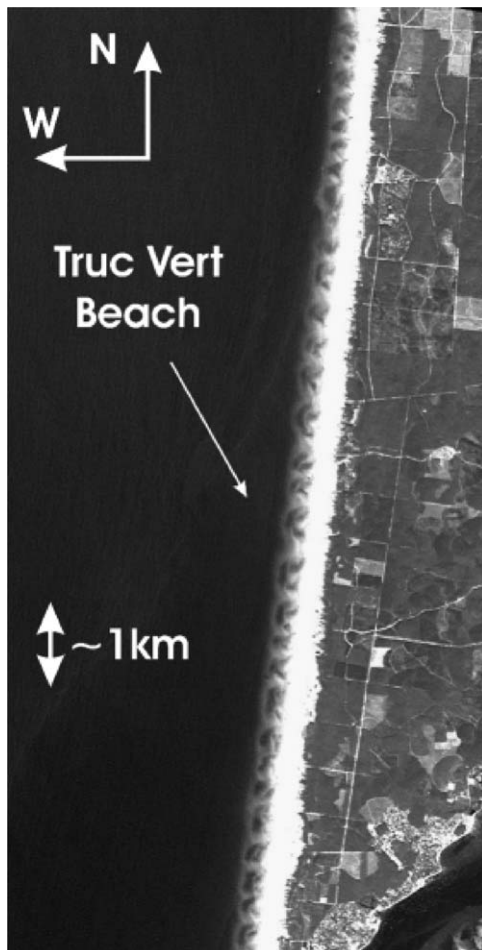


Fig. 3. SPOT image around Truc Vert Beach of regular crescentic bar patterns in the nearshore zone with a mean wavelength of approximately 600 m, SPOT XS1, 15/05/01@CNES-DGO-UMR EPOC.

This nearshore morphology is responsible for complex horizontal water circulations. According to fishermen, lifeguards and surfers, strong tidal modulated rip currents are observed at the runnel outlet, causing several drownings each summer, with maximum flow velocities occurring at mid-tide. This goes against recent studies on other environments (Brander, 1999, 2000) which showed maximum flow velocities occurred at low-tide. Such currents are also responsible for strong water and sediment exchanges between the nearshore and the intertidal zones (Fig. 2). Further offshore, rip currents are also observed over the nearshore crescentic bar systems. For mid- to high-energy conditions, large circulation cells and rip currents are supposed to be induced by waves over this system (Castelle and Bonneton, in press).

In this paper, field measurements of nearshore cell circulation and numerical modelling are combined to investigate the dynamics of waves and wave-induced currents. This study provides the first quantitative description of horizontal circulations on the Aquitanian coast beaches during real conditions.

### 3. Methods

#### 3.1. PNEC 2001 field measurements

A field experiment was conducted at Truc Vert beach on the French Aquitanian coast from the 14th to the 19th of October 2001. The large tidal range allowed instruments to be deployed and recovered safely at low tide while measurements were obtained from mid-tide to high-tide on different swell and tide conditions (Sénéchal et al., 2004). Aerial photographs, satellite images and accurate topography surveys were used to monitor nearshore morphology. The beach profiles were measured at least daily, covering an area extending from the dune to about 200 m offshore, on a longshore distance of about 1 km. The average alongshore spacing between each beach profile was approximately 25 m. A Triaxys directional wave rider moored approximately 15 km off the Cap Ferret on the continental shelf provided incident swell conditions each hour ([http://www.epoc.u-bordeaux.fr/fr/Methys/zone\\_mouillage.html](http://www.epoc.u-bordeaux.fr/fr/Methys/zone_mouillage.html)).

From the 6th to the 9th of October, Truc Vert Beach was exposed to an intense storm. A very energetic quasi-normally incident swell lasted for four days with offshore significant wave heights ranging from 2 to 5 m (Fig. 4). It resulted in a strong

seaward sediment transport and the formation of random direction runnels. The storm was followed by 4 days of relative weak wave conditions resulting in the formation of a berm in the upper part of the beach. The beach area chosen for measurements was strongly alongshore non-uniform and exhibited a ridge and runnel system oriented W–SW in the intertidal domain (Fig. 5). The ridge and runnel system was connected to a small inner crescentic bar system, which can also be defined as a rip head bar following Wright and Short (1984). The nearshore area exhibited an approximately 600 m wavelength crescentic bar system (Desmazes and Michel, 2002). A cusp shape berm was observed in the upper part of the intertidal domain. By the end of the experiment, the beach morphology had changed significantly with the welding of the ridge to the beach face and smoothing of the upper part of the intertidal domain. Quantitatively, between the 16th and the 18th of October, erosion of the berm reached 1.3 m, and the ridge onshore migration was approximately 25 m.

In terms of hydrodynamics, we positioned two cross-shore transects along which four pressure sensors were deployed to provide the alongshore

variability of the cross-shore distribution of wave heights. Three bottom-mounted directional wave current meters were deployed: two S4 InterOcean instruments (S1 and S2 on Fig. 5) positioned at the end of each transect and one Acoustic Doppler Velocimeter (ADV Vector) in between. Instruments were deployed like this in order to study the horizontal circulations over the ridge and runnel systems and to give the alongshore variability of waves and currents. Data were sampled at 8 Hz for the pressure sensors, 2 Hz for the S4 current meters, and 8 Hz for the ADV (Sénéchal et al., 2004). Due to the large tidal range at Truc Vert Beach, the intertidal domain is about 200 m and instruments then can be located alternatively during a tide cycle in the swash, the surf and the shoaling zone.

During the experiment, wave conditions were energetic. Significant wave height ( $H_s$ ) ranged from 1 to 3.1 m (Fig. 4), significant wave period ( $T_s$ ) ranged from 7 to 14 s, with peak swell period reaching 20 s on the 16th. The surf zone was generally wide, reaching a maximum width of 500 m on the 18th. Strong rip currents were observed during medium wave energy conditions at mid-tide at the runnel outlet, and inshore of

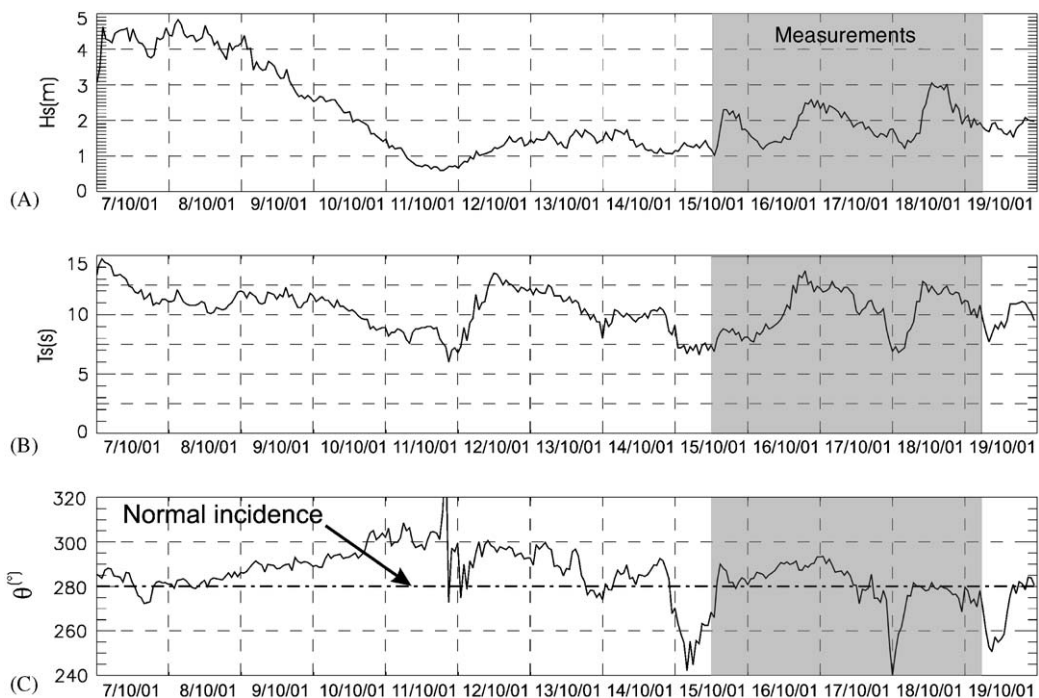


Fig. 4. Offshore wave conditions from eight days before field experiment to the end, the grey area corresponds to the measurement period; (A) Significant wave height  $H_s$ ; (B) significant wave period  $T_s$ ; (C) mean wave incidence  $\theta$ . Data from the Triaxys buoy moored approximately 15 km off the coast.

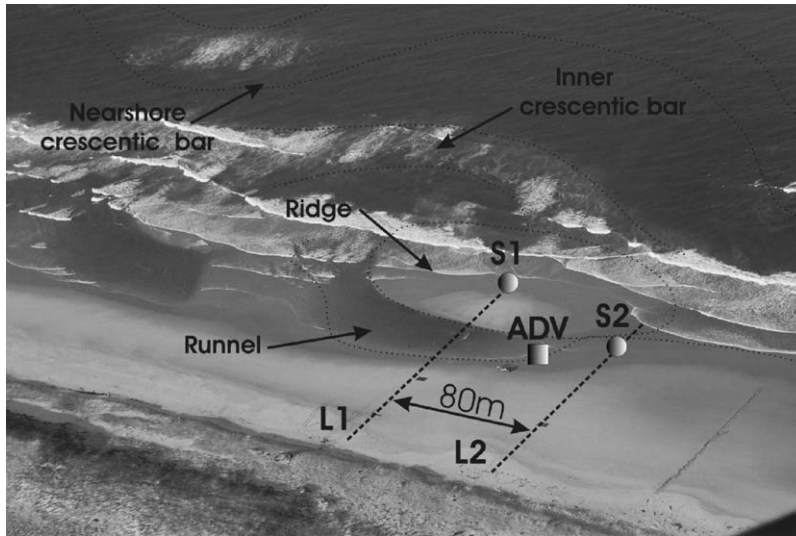


Fig. 5. Section of beach chosen for the field experiment indicating both instrument location and sand bar systems. All instruments are emerged during low tide and immersed during high tide. Two Directional Wave Current Meters S1 and S2, one Acoustic Doppler Velocimeter ADV and two lines of pressure sensors L1 and L2 are shown.

nearshore crescent horns at low tide. The current meters were not positioned near the rip neck in case the instruments were lost.

### 3.2. Numerical model

In this section the equations and underlying assumptions used to model the random wave transformation, the set-up/set-down and the two-dimensional wave-induced current velocities will be briefly presented.

#### 3.2.1. Time- and depth-averaged wave-induced current model

The MORPHODYN model is based on the time average of the depth-integrated mass and momentum conservation equations. The average duration of about 10 min is chosen to be much longer than those for wave groups, but significantly shorter than time scales associated with changes in incident wave conditions. Hydrodynamics are solved using an implicit method to obtain quasi-steady mean water depth  $\bar{h}$  and water volume fluxes  $\bar{Q}_i$ :

$$\bar{Q}_i(x, y, t) = \overline{\int_{Z_f}^{\eta} v_i(x, y, z, t) dz}, \quad (1)$$

where  $(\bar{\cdot})$  is the time average,  $x$  the longshore axis,  $y$  the cross-shore axis,  $z$  the vertical axis,  $v_i$  the water particle velocity,  $Z_f$  the bed elevation and  $\eta$  the free surface elevation. The governing equations are

(Phillips, 1977)

$$\begin{aligned} \frac{\partial \bar{Q}_i}{\partial t} + \frac{\partial}{\partial x_j} \left( \frac{\bar{Q}_i \bar{Q}_j}{\bar{h}} \right) \\ = -g\bar{h} \frac{\partial \bar{\eta}}{\partial x_i} - \frac{1}{\rho} \frac{\partial S_{ij}}{\partial x_j} - \frac{1}{\rho} \frac{\partial R_{ij}}{\partial x_j} + \frac{1}{\rho} \frac{\partial T_{ij}}{\partial x_j} - \frac{\tau_i^b}{\rho}, \end{aligned} \quad (2)$$

$$\frac{\partial \bar{\eta}}{\partial t} + \frac{\partial \bar{Q}_j}{\partial x_j} = 0. \quad (3)$$

In the conservation equations of momentum (2) and mass (3)  $g$  is the gravitational acceleration,  $\rho$  the mass density of water,  $S_{ij}$  the radiation stress components,  $R_{ij}$  the excess of momentum flux due to the wave roller,  $\tau_i^b$  the time-averaged bed stress and  $T_{ij}$  the mixing term.

Wave velocity is separated into two components: a fluctuating velocity  $\hat{v}_i$  (i.e. wave and turbulence) and a mean current velocity  $U_{ci} = U_{ci}(x, y, t)$ :

$$v_i(x, y, z, t) = U_{ci}(x, y, t) + \hat{v}_i(x, y, z, t). \quad (4)$$

According to Phillips (1977) the mean velocity  $U_{ci}$  is defined as

$$U_{ci} = \bar{v}_i. \quad (5)$$

Eqs. (4) and (5) lead to  $\bar{\hat{v}}_i = 0$ ,  $\bar{Q}_i$  can be written as

$$\begin{aligned} \bar{Q}_i &= \overline{\int_{Z_f}^{\eta} U_{ci} dz} + \overline{\int_{Z_f}^{\eta} \hat{v}_i(x, y, z, t) dz} \\ &= \bar{h} U_{ci} + \hat{Q}_i, \end{aligned} \quad (6)$$

where  $\hat{Q}_i$  is the mean volume flux associated with the fluctuating motion. Due to the distinct physical nature of wave and turbulence, the fluctuating velocity  $\hat{v}_i$  can be separated into two components:

$$\hat{v}_i(x, y, z, t) = v'_i(x, y, z, t) + v''_i(x, y, z, t), \quad (7)$$

where  $v'_i$  is the wave fluctuating velocity and  $v''_i$  the turbulence fluctuating velocity. Then  $\hat{Q}_i$  can be decomposed into

$$\begin{aligned} \hat{Q}_i &= \int_{Z_f}^{\eta} v'_i(x, y, z, t) dz + \int_{Z_f}^{\eta} v''_i(x, y, z, t) dz \\ &= \hat{Q}_{wi} + \hat{Q}_{ri}, \end{aligned} \quad (8)$$

where  $\hat{Q}_w$  is the mean volume flux associated with the wave motion and  $\hat{Q}_r$  is the mean volume flux associated with turbulence. The mean current velocity  $U_{ci}$  then becomes

$$U_{ci} = \frac{\hat{Q}_i - \hat{Q}_{wi} - \hat{Q}_{ri}}{\bar{h}}. \quad (9)$$

### 3.2.2. The spectral wave model

For a two-dimensional arbitrary beach topography, the computation of the forcing terms requires the wave field to be specified everywhere. To satisfy this condition, we use the wave program SWAN (Booij et al., 1999) which solves the spectral action balance equation. This wave driver is supposed to simulate accurately the wave field over Aquitanian beaches where reflection and diffraction are not significant (Ris et al., 1998). Triad interaction is taken into account in the computations, but wave–current and quadruplet interactions are not included in the wave modelling.

The breaking wave model chosen herein is the bore-based model of Battjes and Janssen (1978) with a constant breaker parameter  $\gamma = 0.73$  following Battjes and Stive (1985). We apply the bottom friction formulation given by Madsen et al. (1988), which defines the bottom friction coefficient  $C_{Madsen}$  as

$$C_{Madsen} = f_w \frac{g}{\sqrt{2}} U_{rms}, \quad (10)$$

where  $U_{rms}$  is the root-mean-square value of the orbital motion near the bottom, and  $f_w$  is a non-dimensional friction factor estimated by using the formulation of Jonsson (1966):

$$\frac{1}{4\sqrt{f_w}} + \log_{10} \left[ \frac{1}{4\sqrt{f_w}} \right] = m_f + \log_{10} \left[ \frac{a_b}{K_N} \right], \quad (11)$$

where  $m_f = -0.08$ ,  $a_b$  is a representative near-bottom excursion amplitude, and  $K_N$  the bottom roughness length scale.

The driving terms of the hydrodynamic model are computed from the SWAN outputs:  $H_{rms}$ , the mean wave direction  $\theta$ , and the mean wave period  $T$ . The roller area in the surf zone is estimated following Kuriyama and Nakatsukasa (2000). According to Dally (2001), the roller terms are written as

$$\hat{Q}_{ri} = \frac{1}{\rho} \left( \frac{\rho_r A}{T} \right) \frac{k_i}{k}, \quad (12)$$

$$R_{xx} = c \left( \frac{\rho_r A}{T} \right) \left( \cos^2 \theta + \frac{1}{2} \right), \quad (13)$$

$$R_{yy} = c \left( \frac{\rho_r A}{T} \right) \left( \sin^2 \theta + \frac{1}{2} \right), \quad (14)$$

$$R_{xy} = c \left( \frac{\rho_r A}{T} \right) \cos \theta \sin \theta, \quad (15)$$

where  $\rho_r$  is the mass density of the roller,  $C$  is the phase velocity and  $k_i$  is the mean wave number. In shallow water the wave motion is characterized by weak advection of fluid particles. The linear theory gives the volume flux associated with the organized wave motion  $Q_{wi}$  and the random wave energy  $E$ :

$$\hat{Q}_{wi} = \int v'_i dz = \frac{1}{8} \frac{g H_{rms}^2 k_i}{c k} = \frac{E k_i}{\rho c k}, \quad (16)$$

$$E = \frac{1}{8} \rho g H_{rms}^2. \quad (17)$$

The radiation stress components  $S_{ij}$  associated with wave motion are given by Svendsen and Petrevu (1996):

$$S_{ij} = \frac{E}{2} \left\{ \frac{k_i k_j}{k^2} \frac{2C_g}{C} + \delta_{ij} \left( \frac{2C_g}{C} - 1 \right) \right\} - \rho \frac{\hat{Q}_i \hat{Q}_j}{\bar{h}}, \quad (18)$$

where  $C_g$  is the group velocity.

The eddy viscosity  $v_t$  associated with mixing  $T_{ij}$  is determined using combination of a constant eddy viscosity  $v_0$  and the formulation of Battjes (1975), which assumes that mixing in the surf zone is primarily due to the turbulence generated by breaking waves.

$$v_t = Mh \left( \frac{D}{\rho} \right)^{1/3} + v_0, \quad (19)$$

where  $D$  is the rate of energy loss due to depth-induced breaking for the organized wave motion and  $M$  is a dimensionless coefficient.

The final part of the closure problem is the determination of the bed shear stress  $\tau_i^b$ , which is a crucial element in the prediction of horizontal circulations. According to the weak flow approximation (Liu and Dalrymple, 1978), the bottom shear stress due to wave and currents is

$$\tau_i^b = \rho C_f U_w U_{ci}, \quad (20)$$

where  $U_w$  is the bottom oscillatory velocity and  $C_f$  the spatially constant bottom friction coefficient.

This coupled numerical model computes both wave and wave-induced currents. To apply this model to field data, two-dimensional bathymetry and offshore incident wave conditions are required. With these inputs, the model can predict wave characteristics and quasi-steady currents across the entire nearshore zone.

### 3.3. Model inputs

Each hour the offshore wave rider buoy computed the directional wave spectrum, which was used as an offshore boundary condition for the SWAN model. First, the wave field was computed from the wave buoy to 9 m under the Lowest Astronomical Tide (LAT) level. Waves and currents were computed on a refined grid from the 9 m depth isobath to the shoreline on the beach area chosen for the field experiment. The buoy location and the two computational grids used for simulations are

shown in Fig. 6. The bathymetry of the continental shelf was provided by the SHOM (Service Hydrographique et Océanographique de la Marine). The size of the regular computational grid is  $40 \times 80$ , with 400 m mesh steps. The numerical bathymetry of the beach area was derived from the topographic survey of the intertidal domain undertaken on the 16th, and from the 16th satellite SPOT image for the subtidal zone. It is extended to a periodic bathymetry (wavelength equal to a crescent length: 600 m), enabling computation of the mean current field. The computational grid consists of 10 meshes with periodic lateral boundary conditions in the longshore direction.

During the experiment, static water pressures were converted to water surface elevation, and for each sensor the root-mean-square wave height  $H_{rms}$  was estimated from a zero down-crossing analysis, defined as  $H_{rms} = (\sum_{i=1}^n H_i^2)^{1/2} / n$ . Measurements were not taken when the mean water depth ( $\bar{h}$ ) is less than 70 cm, i.e. when they are positioned around the wave trough and occasionally emerge. Root-mean-square wave heights and current velocities were computed each hour over 30-min intervals during the experiment concurrent with the Triaxys buoy data input. During the 18th of October, energetic wave conditions were responsible for a strong morphological evolution of the beach area. Consequently, the last 30 h of measurements is not taken into account because the

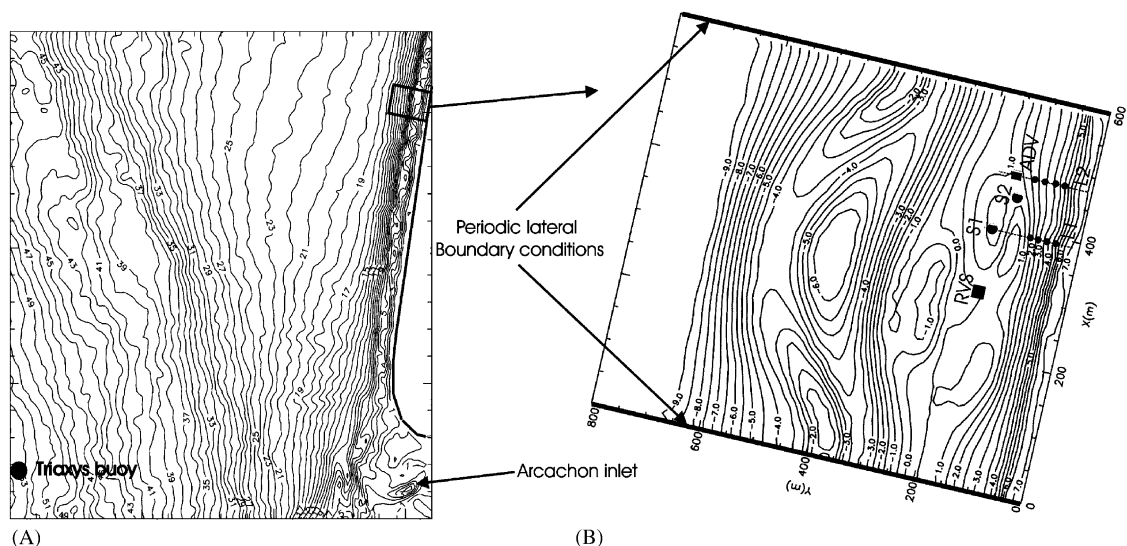


Fig. 6. Coupling of the two numerical bathymetries used for the computation. Bathymetry of the Aquitanian shelf off the field experiment area (copyright SHOM) with the Triaxys buoy location (A), and periodic lateral boundary condition bathymetry of the measurement site, with instrument locations (B).

numerical bathymetry was not accurate enough. Wave heights were computed on the beach area, and the bottom roughness length scale  $K_N$  (Eq. (11)) on the continental shelf was calibrated using the most seaward sensor data (S1). Then hydrodynamic free parameters of MORPHODYN  $C_f$ ,  $v_0$  and  $M$ , are tuned to give the best agreement of the simulations with field data in the nearshore zone.

## 4. Results

### 4.1. Data

During the experiment, measured mean currents ranged from 0.05 to 1.2 m/s, with instantaneous

velocities often reaching 3 m/s (Castelle and Bonneton, 2002). The experiment was characterized by two distinct swell classes. The first (during the three first days of the experiment) is characterized by incident swell at about  $10^\circ$  to the beach, and generating a southward longshore current with a peak of approximately 1 m/s. The second (on the 18th) is characterized by an energetic swell with a shore-normal incidence generating circulation cells and rip currents.

Fig. 7 shows the 150 min time series at station S1, located in the breaker zone, of the low pass filtered signals (frequency cut-off: 0.01 Hz) of water depth  $h$ , cross-shore and longshore velocities during the 17th of October. This period was characterized by offshore incident waves at about  $8^\circ$  to the beach

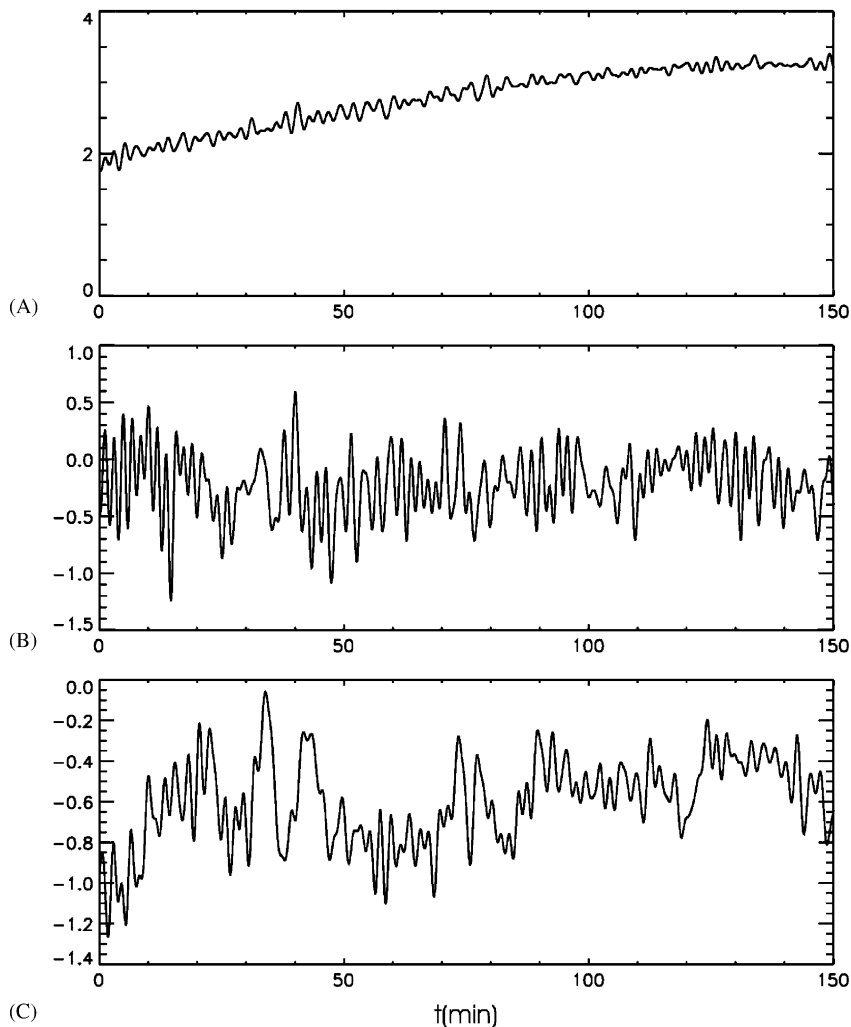


Fig. 7. Times series of 150 min on the 17th of October ( $t_0 = 1\text{h}00$ ) at station S1 of low-passed filtered signals (cut-off frequency 0.01 Hz) of (A) water depth (m); (B) cross-shore velocities (m/s); (C) longshore velocities (m/s).

with root-mean-square wave height  $H_{rms}$  of about 2 m resulting in the generation of a southward longshore current on the order of 0.5–1 m/s. Unsteady longshore flows are observed (Fig. 7), with two strong low frequency modulations: infragravity wave motions (0.004–0.01 Hz) (Bonneton et al., in press), and very low frequency motions (frequencies less than 0.004 Hz). Quasi-steady and unsteady cross-shore flows are weaker, which means longshore current was predominant during this period. Fig. 8 shows the energy spectra associated of the surface elevation  $h$ , cross-shore and longshore velocities during the same period. This figure shows the peak wave energy frequency was about 0.06 Hz (peak wave period of approximately 17 s), while a large amount of longshore velocity energy was

located in the infragravity and far infragravity bands ( $<0.01$  Hz).

Very low frequency motions are obvious during the 18th. Fig. 9 shows the 150 min time series at station S2, located in the breaker zone, of the low pass filtered signals (frequency cut-off: 0.01 Hz) of water depth  $h$ , cross-shore and longshore velocities during the 18th of October. Measured longshore velocities inside the surf zone fluctuate aperiodically with temporal scales of approximately 30 min. This kind of very low frequency motions has been associated with rip current instabilities (Haller and Dalrymple, 2001), but recent studies show that very low frequency surf zone eddies forced by waves are responsible for these low frequency motions (MacMahan et al., 2004). These data confirm that

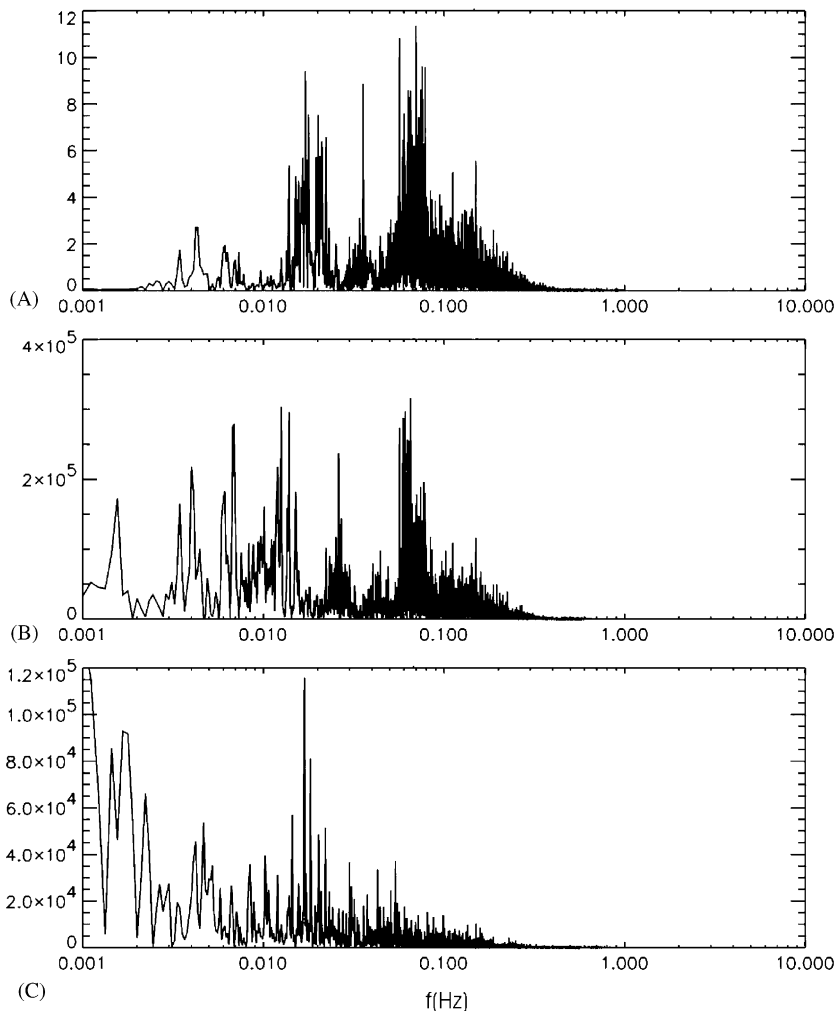


Fig. 8. Energy spectra at station S1 for the time series presented in Fig. 7. (A) Water depth ( $\text{m}^2/\text{Hz}$ ); (B) cross-shore velocities ( $\text{m/s}^2/\text{Hz}$ ); (C) longshore velocities ( $\text{m/s}^2/\text{Hz}$ ).

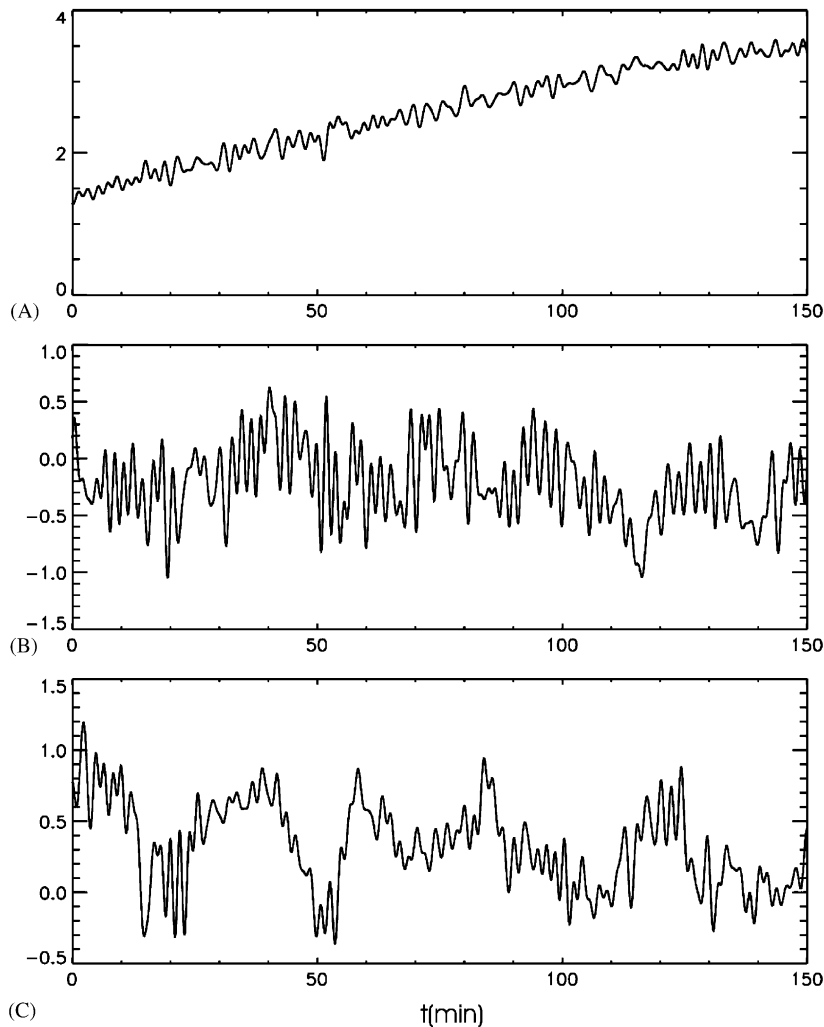


Fig. 9. Times series of 150 min on the 18th of October ( $t_0 = 15\text{h}00$ ) at station S2 of low-passed filtered signals (cut-off frequency 0.01 Hz) of (A) water depth (m); (B) cross-shore velocities (m/s); (C) longshore velocities (m/s).

the amount of very low frequency motion energy increases with swell energy.

These data show the strong control of offshore wave conditions on wave-induced current velocities. A significant amount of velocity energy is in the very low frequency band.

## 4.2. Comparison of field data and model output

### 4.2.1. Waves

The input directional wave spectrum, given by the Triaxys buoy, is specified as the offshore boundary condition of our model. The comparison between computed  $H_{rms}$  and measured  $H_{rms}$  showed scattered results (Fig. 10A). Analysis of meteorological data clearly indicates that the results were most

scattered when the wind was the strongest. Therefore for the calibration of  $K_N$ , only the measurements performed during periods of weak wind and wind sea were taken into account. Particularly, during the 16th of October a long and energetic long swell occurred with non-existent wind, which permitted us to accurately calibrate bottom friction. Then computed and measured wave heights were compared at the S1 location. Best agreement with field data is obtained using  $K_N = 0.085$  for the Madsen model of bottom friction, while the default value in SWAN was  $K_N = 0.05$ . Fig. 10 shows the comparison of the root-mean-square wave height  $H_{rms}$  measured and computed for  $K_N = 0.085$ , for the entire experiment and during weak wind conditions. For the whole experiment, the model is

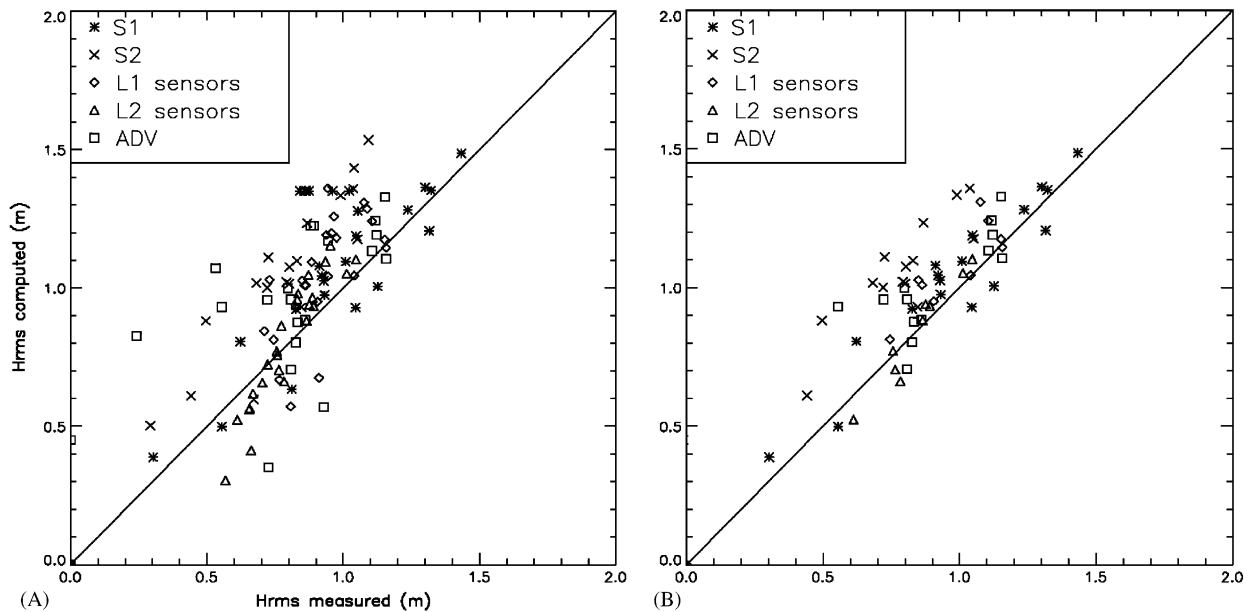


Fig. 10. Comparison between root-mean-square wave height  $H_{rms}$  measured and computed at all the sensor locations, for the whole experiment (A), and during weak wind conditions (B).

in agreement with field data for S1 while the model is less accurate at the other pressure sensor locations deployed on the upper part of the beach. Results are scattered and the model often overestimates wave heights. When only measurements during weak wind conditions are used, the model fits very well with field data for S1, and with good agreement for the other sensors inside and outside the surf zone.

#### 4.2.2. Wave-induced currents

The driving terms of the hydrodynamic module were computed from SWAN outputs. To test the ability of the model to accurately simulate wave-induced currents in the nearshore zone, the value of the depth-averaged longshore current  $U_{cx}$  is compared with the measured longshore currents. We assume that the longshore current velocity measured by current meter (located about 30 cm up to the bottom) is representative of the depth-averaged current velocity. This assumption cannot be applied to the cross-shore current, because its vertical variations are much more important than for the longshore current. The spatially constant bottom friction coefficient  $C_f$  which controls the strength of the wave-induced currents is tuned, and mixing terms  $v_0$  and  $M$ , which control the shape of horizontal circulations and cross-shore thickness of

longshore current. Best agreement with field data during weak wind conditions is found for  $C_f = 0.0048$ ,  $v_0 = 10$  and  $M = 5$ . The value of lateral mixing is an order of magnitude larger than for Ozkan-Haller and Kirby (1999) because a large part of low frequency motions are filtered herein. The value of the bottom friction coefficient  $C_f$  is almost within the range of value given by Whitford and Thornton (1996). Fig. 11 shows the comparison between the mean longshore current  $U_{cx}$  measured and computed for the whole experiment and for only weak wind conditions. We can observe from Fig. 11 that the results are scattered for the whole experiments. However, the model fits very well with field data during weak wind conditions, considering the mathematical approximations of the model and the fact that the wave field was computed 15 km off Truc Vert beach.

Fig. 12 shows simulated two-dimensional current patterns and the comparison of  $H_{rms}$  and  $U_{cx}$  with field data on the crossshore transects L1 and L2 on the 16th of October averaged between 16h30 and 17h00. During this day, the wind and the wind sea were non-existent, and an energetic, long and narrow banded swell occurred (peak swell period between 16 and 20 s). All day long, the model fits very well with measurements for the wave height and the longshore current. A relevant feature of

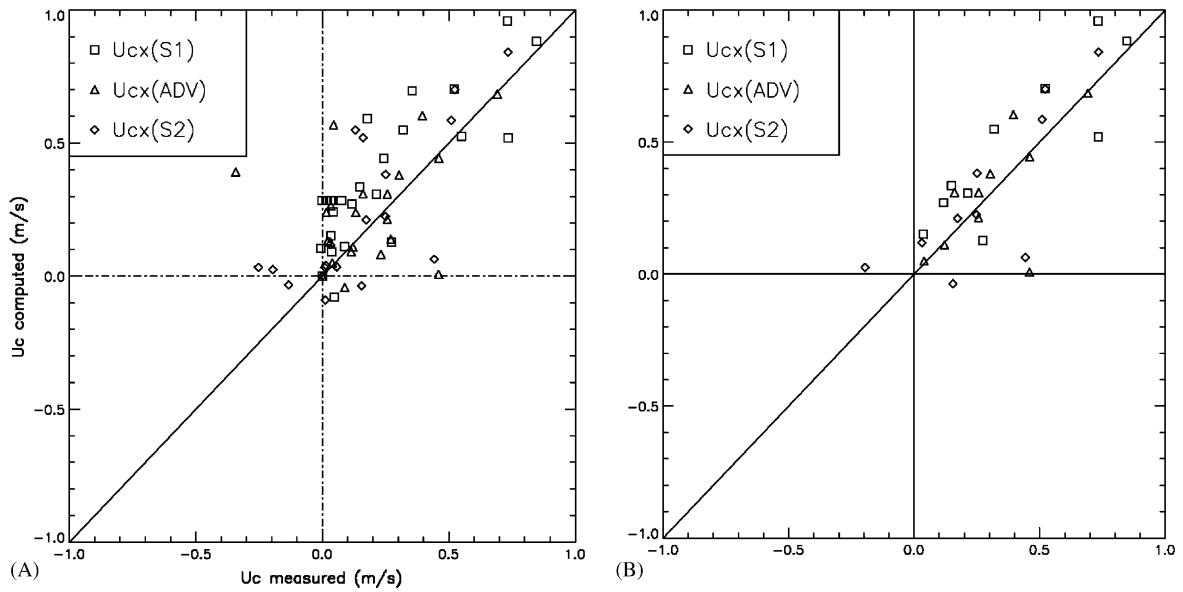


Fig. 11. Comparison between the longshore current ( $U_{cx}$ ) measured and computed, for the whole experiment (A), and during weak wind conditions (B). Model free parameters:  $C_f = 0.0015$ ,  $v_0 = 10$  and  $M = 5$ .

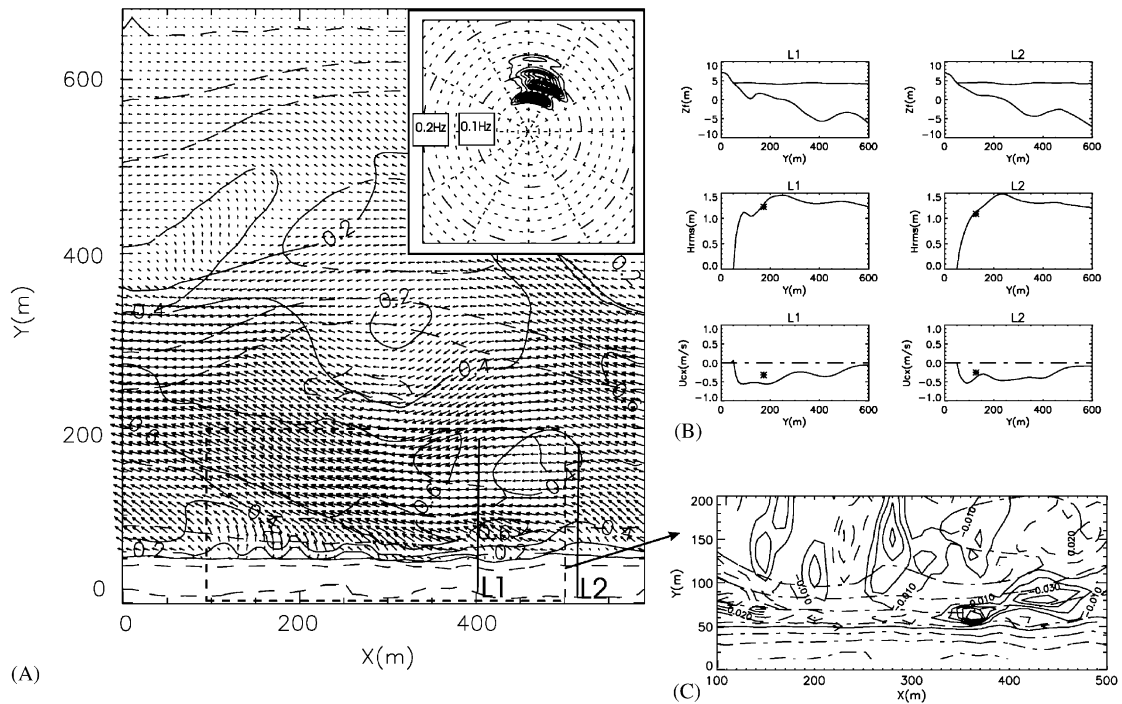


Fig. 12. (A) Simulation of mean wave-induced current  $\bar{U}_c$  over the PNEC 2001 bathymetry the 16th of October 2001 (time-averaged between 16h30 and 17h00) with the directional wave spectrum given by the Triaxys wave rider. The solid lines represent the iso-values of mean current velocities  $\bar{U}_c$  in m/s and the dashed lines correspond to the bathymetry (2 m contour, concurrent with the thick line of Fig. 6). (B) Comparison of the model results with field data at the cross-shore transects L1 and L2 for the mean longshore current  $\bar{U}_{cx}$  and root-mean-square wave height  $H_{rms}$ . (C) Zoom of the longshore pressure gradient field  $-\rho g h (\partial \bar{\eta} / \partial x)$  inshore the ridge and runnel system.

simulations is the location of the maximum longshore current in the bar trough (Fig. 12B). This is due to longshore pressure gradients induced by the fully three-dimensional behaviour of the beach area (Fig. 12C). These longshore pressure gradients inshore of the ridge and runnel system induce an intensification of the longshore current in the runnel.

It was found that results are correct for strong longshore current velocities, but are less accurate for low longshore current with velocity smaller than 0.4 m/s. It is possible that our computational grid is not accurate enough to reproduce under-scaled phenomena, which can be predominant under low energy conditions.

### 4.3. Horizontal circulation patterns over the ridge and runnel system

#### 4.3.1. Background

Both the ridge and runnel system and the nearshore crescentic bar are responsible for complex horizontal circulations depending on the tide level and the offshore wave conditions. Castelle and Bonneton (in press) investigated the circulations induced by the nearshore crescentic bar system. They showed that circulation cells and strong rip currents occurred in intertidal and subtidal zones, with strong tidal modulation of surf zone processes. The sensitivity of the horizontal circulation, and especially the rip current behaviour at the runnel outlet, to the tide level and the offshore wave conditions will be investigated.

Rip currents are common on beaches exhibiting three-dimensional topography and exposed to normal or near-normal incident swells (Aagaard et al., 1997; Brander, 2000). Rip cell circulations are controlled by topographic feed-back and are supposed to be responsible for strong water and sediment exchanges between the surf zone and the nearshore zone (Short, 1985), resulting in a strong influence on the beach morphology. On the Aquitanian coast, these rip currents occur at each runnel outlet and their intensity depends on the length, the shape of the system, the offshore wave conditions and the tide level. No current meter was placed in the rip neck during the field measurement, and no previous data are available in rip currents in these environments. However, tidal modulation is known by locals to occur with maximum rip velocities occurring more or less at mid-tide. The mechanism leading to the formation of a rip current

can be summarized studying the ridge and runnel system during the PNEC 2001 field measurements. Let us assume that incoming wave field is longshore uniform. Waves approaching the bar will break before waves approaching the runnel, the induced set-up in the runnel will then begin further inshore, inducing longshore pressure gradients inshore the ridge and runnel system. These longshore pressure gradients drive the feeder currents which lead to a rip current system associated with horizontal circulation cells. These longshore pressure gradients have been successfully measured in laboratory (Haller and Dalrymple, 1999), and more recently in the field (Haas et al., 2002).

#### 4.3.2. Simulation of a rip current

Fig. 13 shows the two-dimensional current patterns simulated during a normally incident swell on the 18th of October 2001. A strong narrow, seaward oriented current (maximum mean flow on the order of 1 m/s) is located at the runnel outlet, associated with a large circulation cell. The onshore flow of this circulation is located on the bar and is broader and weaker, on the order of 0.5 m/s. The computed longshore pressure gradient field  $-\rho gh(\partial\bar{\eta}/\partial x)$  over the ridge and runnel system during the same period is given in Fig. 13B. On the upper part of the beach (less than 1 m water depth), the longshore pressure gradients force the feeder currents. Water convergence inshore the runnel outlet results in the formation of a seaward oriented current which balances the water mass conservation equation inshore the runnel outlet. The computed rip current system is in agreement with the Lagrangian rip flow measurements of Brander (1999): flow velocities at the base of the feeders are relatively weak and quickly increase in the body of the rip up to 0.9 m/s before decreasing in the rip head.

#### 4.3.3. Model to data comparison

For normal to near-normal incoming swells, rip currents are always associated with circulation cells. The wave-induced currents on the bar are also tidally modulated because they are associated with the broad flow of the circulation cell. Fig. 14 shows the variations of the mean current  $U_{cx}$  during two tidal cycles from mid-tide to high-tide on the 16th of October, for a wave incidence of about  $6^\circ$ . This figure shows the tidal modulation of mean longshore flow measured at S1 and S2, with stronger currents at mid-tide. The tidal modulation on the

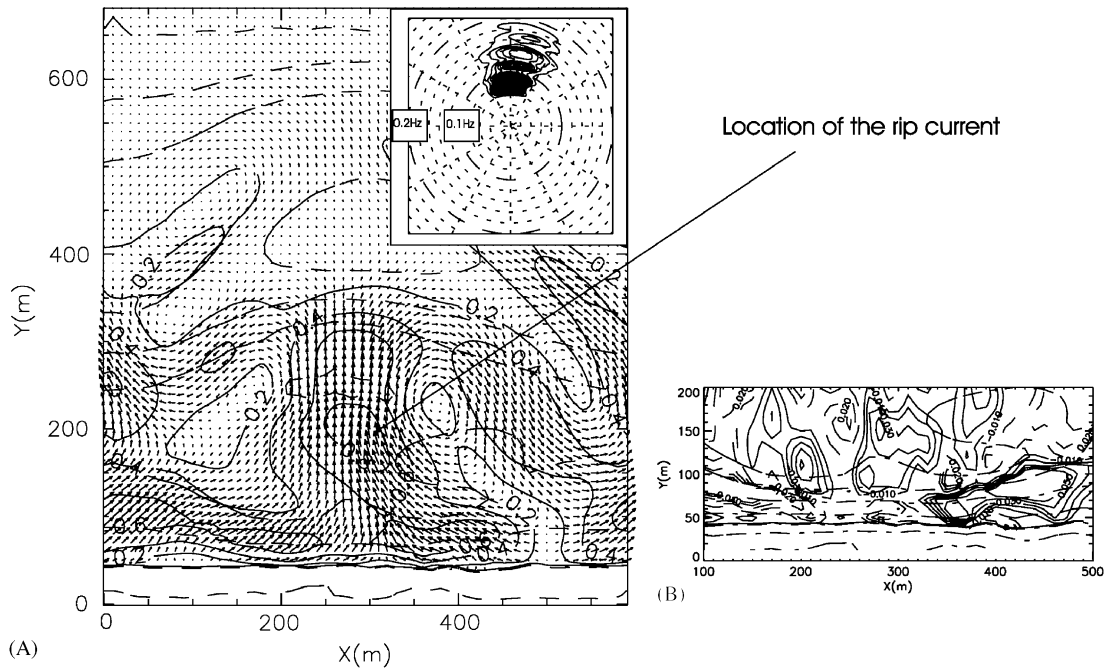


Fig. 13. Simulation of mean wave-induced current  $\bar{U}_c$  over the PNEC 2001 bathymetry during a frontal swell  $H_s = 3$  m at mid-high tide, the 18th of October 2001, 15 h (with the directional wave spectrum given by the Triaxys wave rider). The solid lines represent the iso-values of mean current velocities  $\bar{U}_c$  in m/s and the dashed lines correspond to the bathymetry (2 m contour, concurrent with the thick line of Fig. 6). Visualization of a strong and narrow seaward oriented rip current which maximum flow velocity is located at the runnel outlet. (B) Zoom of the longshore pressure gradient field  $-\rho g h (\partial \eta / \partial x)$  inshore the ridge and runnel system.

bar (station S1) is stronger than the modulation measured on the side of the bar (station S2). The model reproduces this tidal modulation very well (Fig. 14), except for the peak velocity at 17h30, with a good sensitivity to the increasing offshore wave conditions.

#### 4.3.4. Model analysis

Simulations with stationary offshore wave conditions during one tidal cycle are required for a better understanding of this rip current. A virtual sensor station VS was defined at the runnel outlet where strong rip current velocities are supposed to occur. Incident wave angle is the main offshore wave characteristic controlling rip current shape. On October 16 at 15 h (Fig. 12) the  $8^\circ$  incoming swell is responsible for a strong longshore current from the shoreline to about 400 m offshore and no circulation cell or rip current is observed. For normal incidence swell the rip is oriented seaward, very intense and confined. Normally incident swells are used for the rip current simulations.

Wave period controls strength and shape of the rip currents. Indeed, longer swells lead to stronger

and narrower rip currents (Fig. 15). Longer swells induce stronger spatial radiation stress gradients which force more intense circulation cells. For  $T_p = 12$  s, rip velocity at station VS is almost double than for  $T_p = 6$  s. For  $T_p > 14$  s the rip velocity lightly decreases with increasing wave period.

Offshore wave height is the main wave characteristic controlling the rip velocities. Fig. 16 shows the location of the virtual sensor VS and the simulations of rip current velocities  $U_c$  at the station VS during one tidal cycle for normally incident swell with significant wave heights  $H_s$  ranging from 0.5 to 2 m. Results reveal that maximum rip current velocity occurs between mid-tide and high-tide. For  $H_s$  up to 2 m the maximum of rip velocity occurs at high-tide, while it occurs at mid-tide for  $H_s = 1$  m. Changes in the breaking pattern control the rip current characteristics. From mid-low tide to high-tide, waves are breaking on the ridge and runnel system, which leads to a longshore pressure gradient inshore then inducing the rip current. During a tidal cycle, the temporal occurrence of maximum rip current velocity depends on both the longshore pressure

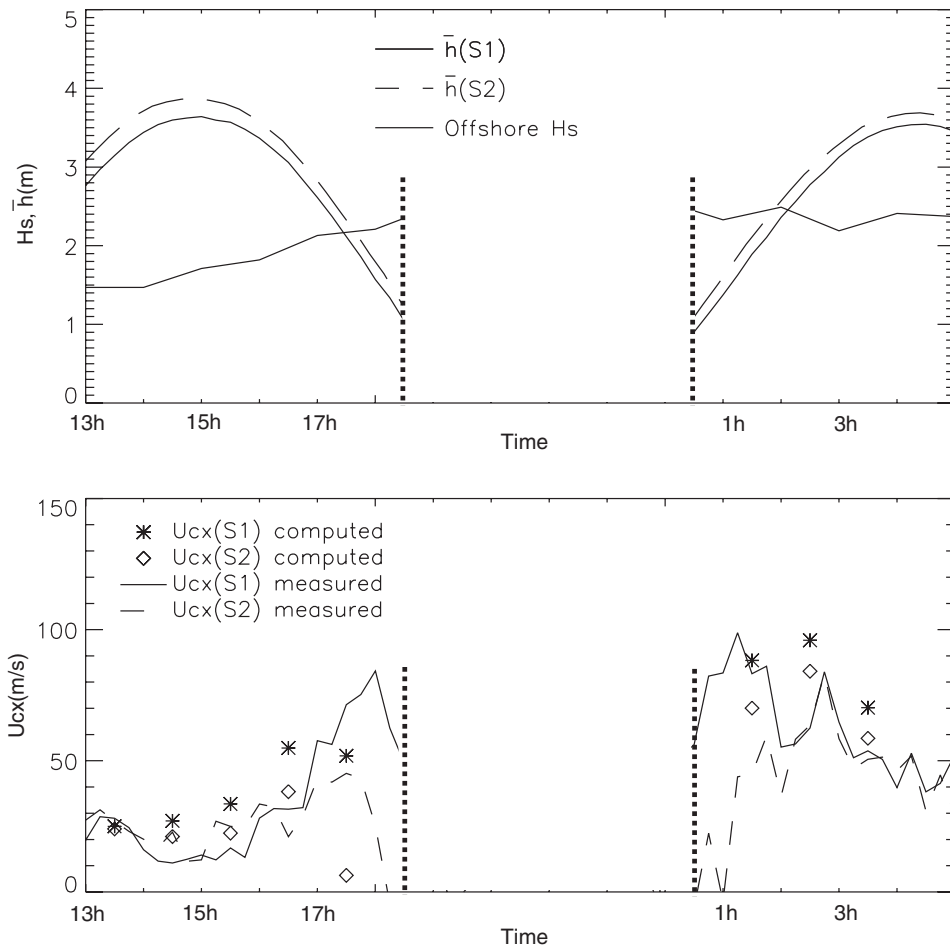


Fig. 14. Comparison between the longshore current  $\bar{U}_{cx}$  measured and computed during two tide cycles, with offshore significant wave height  $H_s$  and mean water level  $\bar{h}$  at stations S1 and S2. The 16th of October 2001.

gradient intensity inshore the ridge and runnel system and the cross-sectional area of the runnel outlet available for rip flow.

Consequently, it appears that the ridge and runnel morphology is a key parameter for rip current characteristics and especially the temporal occurrence of maximum flow velocities. Comparison with other rip studies reveals the Aquitanian coast rip currents behave differently from rip systems in low-energy environments (Aagaard et al., 1997; Brander, 1999), or other case studies in high energy environments (Brander, 2000). The morphology of these environments strongly differs from the Aquitanian coast beach morphology. The main reason is that the Aquitanian ridge and runnel system is almost uncovered at low-tide, and totally uncovered at spring low-tide, and thus cannot enable longshore pressure gradients likely to drive feeders.

## 5. Conclusion

Field measurements of waves and longshore currents were obtained on a ridge and runnel system at Truc Vert Beach under a range of incident wave conditions. Field data were compared with a time- and depth-averaged numerical model formulated for an irregular wave field. Computed offshore root-mean-square wave heights are in good agreement with field data inside and outside the surf zone during weak wind conditions. Considering the mathematical approximations involved, the model fits well with data and quantitatively simulates the tidal modulation of flow velocities on the bar.

A first description of the dynamics of wave-induced currents on Aquitanian ridge and runnel systems has been done. Longshore pressure gradients induced are responsible for the location of maximum longshore currents in the trough and

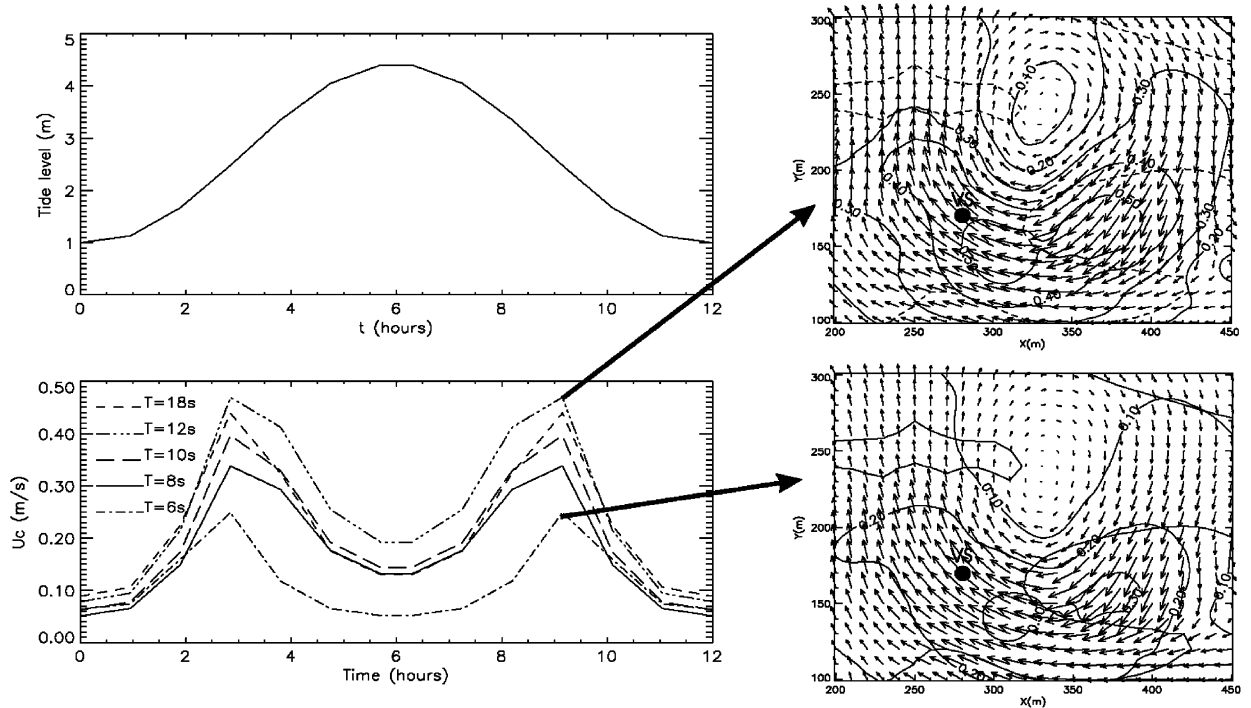


Fig. 15. (A) Tide cycle used for the simulations. (B) Simulation of rip current velocities  $U_c$  at VS during one tide cycle; boundary wave conditions: normal incoming swell,  $H_s = 1$  m, different wave period  $T$ . (C) Zoom of the rip current feature for  $T = 6$  s. (D) Zoom of the rip current feature for  $T = 12$  s.

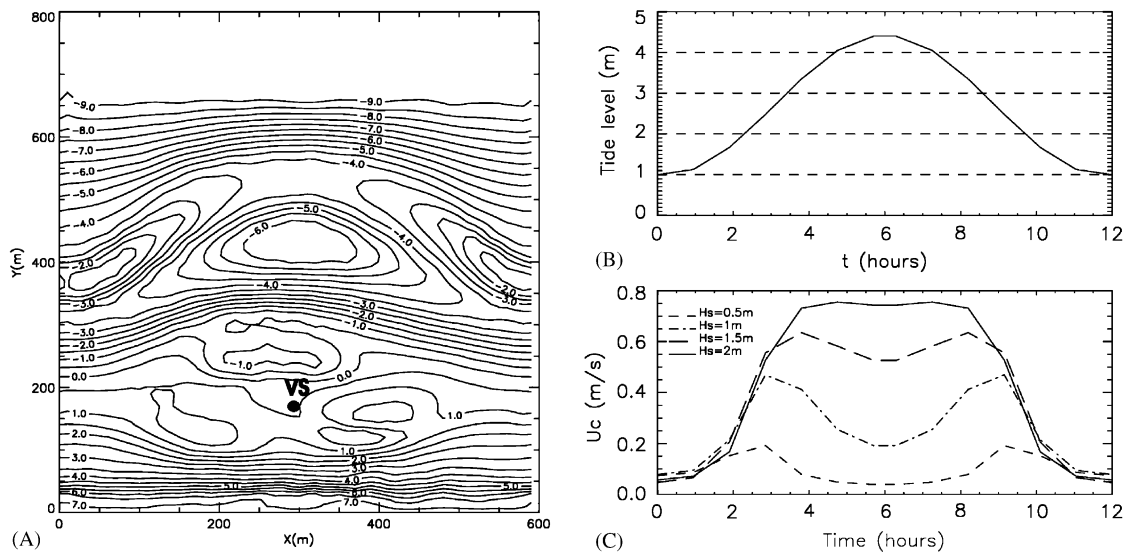


Fig. 16. (A) Location of the virtual station VS on the PNEC 2001 bathymetry. (B) Tidal cycle used for the simulations. (C) Simulation of rip current velocities  $U_c$  at VS during one tide cycle; offshore wave conditions: normal incoming swell, mean wave period  $T = 10$  s, significant wave heights  $H_s$  ranging from 0.5 and 2 m.

drive the feeder which leads to rip currents. This paper emphasizes both the tidal modulated behaviour of the rip velocities and rip current sensitivity to offshore wave conditions. Results show that

maximum rip current flows occur at mid-tide which differs from previous results observed in other beach environments. A strong coupling exists between bed morphology and hydrodynamics.

Results would be quite different for developed ridge and runnel system like those observed at the end of summer, just before the September first energetic swells.

This study constitutes the first stage of knowledge of the dynamics of waves and currents on the Aquitanian high energy beaches. It puts in evidence some mechanisms which should be investigated in more detail during further experiments. Further investigations (modelling and measurements) on different ridge and runnel morphologies are required for a full understanding. Given the strong currents observed on the Aquitanian coast beaches, wave–current interaction also has to be included in the modelling approach.

### Acknowledgements

This study was performed within the framework of the Programme National d'Environnement Côtier, project “Hydrodynamique sédimentaire en zone côtière”, sponsored by the CNRS/INSU. Bruno Castelle was financially supported by EP-SHOM and DGA for his Ph.D. studies. The authors would like to thank G. Oggian, F. Desmazes, H. Howa, V. Rey, D. Rihouey, C. Brière, S. Abadie, V. Rey, R. Pedreros, P. Larroude among others for their help and support during PNEC2001 field measurements. We acknowledge the constructive criticism by R. W. Brander and an anonymous reviewer which significantly improved the contents of the paper.

### References

- Aagaard, T., Greenwood, B., Nielsen, J., 1997. Mean currents and sediment transport in a rip channel. *Marine Geology* 140, 25–45.
- Battjes, J., 1975. Modelling of turbulence in the surf zone. In: *Symposium on Modeling Techniques*, ASCE, pp. 1050–1061.
- Battjes, J., Janssen, J., 1978. Energy loss and set-up due to breaking of random waves. In: *Proceedings of the 16th International Conference on Coastal Engineering*, ASCE, pp. 569–587.
- Battjes, J., Stive, M., 1985. Calibration and verification of a dissipation model for random breaking waves. *Journal of Geophysical Research* 90 (C5), 9159–9167.
- Bonneton, P., Mariou, V., Dupuis, H., Sénéchal, N., Castelle, B. Wave transformation and energy dissipation model for random breaking waves. *Journal of Coastal Research* SI 39, in press.
- Booij, N., Ris, R., Holthuijsen, L., 1999. A third-generation wave model for coastal regions, part i: model description and validation. *Journal of Geophysical Research* 104 (C4), 7649–7666.
- Brander, R., 1999. Field observations on the morphodynamic evolution of low-energy rip current system. *Marine Geology* 157, 199–217.
- Brander, R., 2000. Morphodynamics of a large-scale rip current system at Muriwai Beach, New Zealand. *Marine Geology* 165, 27–39.
- Butel, R., Dupuis, H., Bonneton, P., 2002. Spatial variability of wave conditions on the French Aquitanian Coast using in-situ data. *Journal of Coast Research* SI 36, 96–108.
- Castelle, B., Bonneton, P., 2002. Wave-induced currents over the Aquitanian Coast sand bars. In: *8th International Symposium on Oceanography of the Bay of Biscay*.
- Castelle, B., Bonneton, P. Nearshore waves and currents over crescentic bars. *Journal of Coast Research* SI 39, in press.
- Castelle, B., Bonneton, P., Dupuis, H., Michel, D., Howa, H., Sénéchal, N. The French Aquitanian Coast: a high energy environment. *Marine Geology*, submitted.
- Church, J., Thornton, E., 1993. Effects of breaking wave induced turbulence within a longshore current model. *Coastal Engineering* 20, 1–28.
- Cook, D., 1970. The occurrence and geologic work of rip current off Southern California. *Marine Geology* 9, 173–186.
- Dally, W., 2001. Modeling nearshore currents on reef-fronted beaches. In: *Proceedings of Coastal Dynamics*.
- Davies, J., 1980. *Geographical Variation in Coastal Development*, second ed. Longman, London.
- Desmazes, F., Michel, D., 2002. Sedimentation of a high energetic lower shoreface: example of Truc Vert Beach. In: *Proceedings of the 8th International Symposium on Oceanography of the Bay of Biscay*, p. 45.
- Feddersen, F., Guza, R., 2003. Observation of nearshore circulation: alongshore uniformity. *Journal of Geophysical Research* 108 (C1), 15667–15676.
- Feddersen, F., Guza, R., Elgar, S., Herbers, T., 1998. Alongshore momentum balances in the nearshore. *Journal of Geophysical Research* 103 (C8), 15667–15676.
- Froidefond, J.-M., Gallissaires, J.-M., Prud'homme, R., 1990. Spatial variation in sinusoidal on a crescentic nearshore bar: application to the Cap Ferret Coast. *Journal of Coastal Research* 6, 927–942.
- Haas, K., Svendsen, I., 2002. Laboratory measurements of the vertical structure of rip current. *Journal of Geophysical Research* 107 (C5).
- Haas, K., Svendsen, I., Brander, R., Nielsen, P., 2002. Modeling of a rip current system on Moreton Island, Australia. In: *Proceedings of International Conference on Coastal Engineering*, ASCE.
- Haller, M., Dalrymple, R., 1999. Rip currents dynamics and nearshore circulation. Center of Applied Coastal Research, University of Delaware.
- Haller, M., Dalrymple, R., 2001. Rip current instabilities. *Journal of Fluid Mechanics* 433, 161–192.
- Hamilton, D., Ebersole, B., 2001. Establishing uniform longshore currents in a large-scale sediment transport facility. *Coastal Engineering* 42, 199–218.
- Inman, D., Tait, R., Nordstrom, C., 1971. Mixing in the surf zone. *Journal of Geophysical Research* 76 (C15), 3493–3514.
- Jonsson, I., 1966. Wave boundary layers and friction factors. In: *Proceedings of the 10th International Conference on Coastal Engineering*, pp. 109–152.

- Kuriyama, Y., Nakatsukasa, T., 2000. A one-dimensional model for undertow and longshore current on a barred beach. *Coastal Engineering* 40, 39–58.
- Lafon, V., Dupuis, H., Howa, H., Froidefond, J.-M., 2002. Determining ridge and runnel longshore migration rate using spot imagery. *Oceanologica Acta* 25, 149–158.
- Lafon, V., Dupuis, H., Butel, R., Michel, D., Howa, H., De Melo Apoluceno, D., 2005. Rhythmic sub-tidal and inter-tidal bar morphology and dynamics in a mixed-energy environment. Part II: Physical forcing analysis. *Estuarine Coastal and Shelf Science* 65(3), 449–462.
- Liu, P., Dalrymple, R., 1978. Bottom frictional stresses and longshore currents due to waves with large angle of incidence. *Journal of Marine Research* 36, 357–375.
- Longuet-Higgins, M., 1970. Longshore current generated by obliquely incident sea waves. *Journal of Geophysical Research* 75, 6778–6801.
- MacMahan, J., Thornton, E., Stanton, T., Reniers, A., Dean, R., 2003. Ripex: rip-current pulsation measurements. *Coastal Engineering* 2002: Solving Coastal Conundrums, 736–746.
- MacMahan, J., Reniers, A., Thornton, E., Stanton, T., 2004. Surf zone eddies coupled with rip current morphology. *Journal of Geophysical Research* C07004, doi:10.1029/2003JC002083.
- Madsen, O., Poon, Y.-K., Graber, H., 1988. Spectral wave attenuation by bottom friction: theory. In: *Proceedings of the 21st International Conference on Coastal Engineering*, pp. 492–504.
- Michel, D., Howa, H., 1994. Morphological evolution of a littoral sand bank, modelisation of its dynamics. *Annals Geophysical, European Geophysical Union, Part II* 12, 240.
- Michel, D., Howa, H., 1999. Short-term morphodynamic response of a ridge and runnel system on a mesotidal sandy beach. *Journal of Coastal Research* 15, 428–437.
- Ozkan-Haller, H.T., Kirby, J.T., 1999. Nonlinear evolution of shear instabilities of the longshore current: a comparison of observations and computations. *Journal of Geophysical Research* 104 (C11), 953–984.
- Putrevu, U.J., Oltman-Shay, J., Svendsen, I.A., 1995. Effect of alongshore non uniformities of longshore current predictions. *Journal of Geophysical Research* 100 (C16), 119–130.
- Phillips, O., 1977. *The Dynamics of the Upper Ocean*. Cambridge University Press, Cambridge.
- Reniers, A., Battjes, J., 1997. A laboratory study of longshore currents over barred and non-barred beaches. *Coastal Engineering* 30, 1–22.
- Ris, R., Booij, N., Holthuijsen, L., 1998. A third-generation wave model for coastal regions, part ii: Verification. *Journal of Geophysical Research* 104 (C4), 7649–7666.
- Ruessink, B., Miles, J., Feddersen, F., Guza, R., Elgar, S., 2001. Modeling the alongshore current on barred beaches. *Journal of Geophysical Research* 106, 22451–22463.
- Sénéchal, N., Dupuis, N., Bonneton, P., 2004. Preliminary hydrodynamic results of a field experiment on a barred beach, Truc Vert Beach on October 2001. *Ocean Dynamics* 54, 408–414.
- Short, A., 1979. Three-dimensional beach-stage model. *Journal of Geology* 87, 553–571.
- Short, A., 1985. Rip current type, spacing and persistence, Narrabeen Beach, Australia. *Marine Geology* 65, 103–137.
- Short, A., 1992. Beach systems of the Central Netherlands Coast: processes, morphology and structural impacts in a storm driven multi-bar system. *Marine Geology* 107, 103–137.
- Short, A., Aagaard, T., 1993. Single and multi-bar beach change models. *Journal of Coastal Research* SI 15, 141–157.
- Short, A., Brander, R., 1999. Regional variations in rip density. *Journal of Coastal Research* 15 (3), 813–822.
- Sonu, C., 1972. Field observation on nearshore circulation and meandering currents. *Journal of Geophysical Research* 77, 3232–3247.
- Svendsen, I., Petrevu, U., 1996. *Surf-Zone hydrodynamics, Advances in Coastal and Ocean Engineering*, vol. 2. World Scientific, Singapore.
- Visser, P., 1991. Laboratory measurements of uniform longshore current. *Coastal Engineering* 15, 563–593.
- Whitford, D., Thornton, E., 1996. Bed shear stress coefficients for longshore currents over a barred profile. *Coastal Engineering* 27, 243–262.
- Wright, L., Short, A., 1984. Morphodynamic variability of surf zone and beaches: a synthesis. *Marine Geology* 56, 93–118.